

PAPER

# Topotactic transition between perovskite and brownmillerite phases for epitaxial $\text{LaCoO}_{3-\delta}$ films and effects thus resulted

## Recent citations

- [Strain-induced structure and oxygen transport interactions in epitaxial  \$\text{La}\_{0.6}\text{Sr}\_{0.4}\text{CoO}\_3\$  thin films](#)  
Yurii P. Ivanov *et al*

To cite this article: Hailin Huang *et al* 2020 *J. Phys. D: Appl. Phys.* **53** 155003

View the [article online](#) for updates and enhancements.



**IOP | ebooks™**

Bringing together innovative digital publishing with leading authors from the global scientific community.

Start exploring the collection—download the first chapter of every title for free.

# Topotactic transition between perovskite and brownmillerite phases for epitaxial $\text{LaCoO}_{3-\delta}$ films and effects thus resulted

Hailin Huang<sup>1,2</sup>, Jine Zhang<sup>1,2</sup>, Hui Zhang<sup>1</sup>, Furong Han<sup>1,2</sup>,  
Xiaobing Chen<sup>1,2</sup>, Jinghua Song<sup>1,2</sup>, Jing Zhang<sup>1</sup>, Shaojin Qi<sup>1,2</sup>,  
Yuansha Chen<sup>1</sup>, Jianwang Cai<sup>1,2</sup>, Fengxia Hu<sup>1,2,3</sup>, Baogen Shen<sup>1,2,3</sup>  
and Jirong Sun<sup>1,2,3</sup> 

<sup>1</sup> Beijing National Laboratory for Condensed Matter Physics and Institute of Physics, Chinese Academy of Sciences, Beijing 100190, People's Republic of China

<sup>2</sup> School of Physical Sciences, University of Chinese Academy of Sciences, Beijing 100049, People's Republic of China

<sup>3</sup> Songshan Lake Materials Laboratory, Dongguan, Guangdong 523808, People's Republic of China

E-mail: [jrsun@iphy.ac.cn](mailto:jrsun@iphy.ac.cn)

Received 7 November 2019, revised 13 January 2020

Accepted for publication 15 January 2020


Published 7 February 2020



## Abstract

Oxygen vacancy distribution has a direct effect on the crystal structure and physical properties of complex oxides, resulting in versatile applications. Here, we report on a reversible topotactic phase transition between the perovskite and brownmillerite structures for the  $\text{LaCoO}_{3-\delta}$  ( $\delta = 0-0.5$ ) epitaxial film by annealing the sample under different conditions. In the atmosphere of  $2 \times 10^{-4}$  Pa,  $\text{LaCoO}_3$  film is transformed from the perovskite structure to the brownmillerite structure when annealing temperature exceeds 500 °C. Meanwhile, the magnetic order transits from ferromagnetic to anti-ferromagnetic. Variable-range hopping demonstrates the electronic transport process for both phases. The incorporation of oxygen vacancies results in an upward shift of the  $\ln\rho-T^{-1/4}$  curve, without affecting the  $\ln\rho-T^{-1/4}$  slope. We found signatures for preferential distribution for oxygen vacancies; the latter prefer to appear near high spin  $\text{Co}^{3+}$  ions in the initial stage when they are introduced into the lattice, resulting in abnormal magnetic and transport behaviors.

Keywords:  $\text{LaCoO}_3$  film, oxygen vacancy ordering, brownmillerite structure

 Supplementary material for this article is available [online](#)

(Some figures may appear in colour only in the online journal)

## Introduction

Oxygen stoichiometry plays a crucial role in determining the physical properties and potential application of the transition metal oxides (TMOs). A small change in oxygen content can result in a considerable variation of the oxidation state of the transition metal, drastically modifying the functionalities of the oxides [1–14]. A typical example is the brownmillerite (BM)-structured oxides with ordered oxygen vacancies. This phase can be derived from perovskite (PV) TMOs, after a topotactical

transformation in reduced atmospheres, and exhibits unusual magnetic, transport and catalytic properties [6–14]. Many efforts have been devoted to obtaining the derived structure of the PV manganite oxide [6–8], ferrite oxide and cobalt oxide [9–15]. The typical example is the topotactic phase transformation in  $\text{SrCoO}_{3-\delta}$  [11]. It results in a reversible switch between three phases, PV-structured  $\text{SrCoO}_{3-\delta}$  (a ferromagnetic metal), BM-structured  $\text{SrCoO}_{2.5}$  (an antiferromagnetic insulator), and  $\text{HSrCoO}_{2.5}$  (a weak ferromagnetic insulator). The latter is a BM phase with interstitial H ions.

Cobalt oxides usually have excellent ionic conductivity, electronic conduction, and catalytic activity, having many practical applications in fields such as solid oxide fuel cells, rechargeable batteries, gas sensors, and memristive devices [16–21]. Cobalt oxide is one of the most intriguing PV-structure oxides. For example,  $\text{Co}^{3+}$  ion in bulk  $\text{LaCoO}_{3-\delta}$  (LCO) exhibits multiple spin states due to the delicate balance between crystal-field splitting ( $\Delta_{CF}$ ) and Hund's rule coupling ( $J_{ex}$ ) [22–24], namely low spin state (LS,  $t_{2g}^6 e_g^0$ ,  $S = 0$ ), intermediate spin state (IS,  $t_{2g}^5 e_g^1$ ,  $S = 1$ ), and high spin state (HS,  $t_{2g}^4 e_g^2$ ,  $S = 2$ ). Unlike its bulk counterpart, the epitaxial LCO thin film under tensile strains is ferromagnetic (FM) below 85 K, due to the occurrence of the superexchange between HS and LS  $\text{Co}^{3+}$  ions, and insulating with a behavior of three-dimensional (3D) variable-range hopping [25–29]. Recently, a series of investigations on the microscopic structure of epitaxial LCO films have been performed by transmission electron microscopy (TEM) [31–36]. The common observation of these works is the occurrence of the dark stripes in lattice images of tensely strained LCO films, which is a signature for the appearance and ordering of oxygen vacancies. The influence of the density of dark stripes on the FM properties of LCO films was also studied [29–35]. We noticed that the dark stripe patterns observed in the LCO film are quite similar to the TEM results of the BM-structured oxides such as  $\text{SrCoO}_{2.5}$  and  $\text{SrFeO}_{2.5}$ , which is due to the alternate  $\text{CoO}_4$  layers sandwiched between the  $\text{CoO}_6$  layers [9–14]. However, as the TEM results only reflect the characteristics of very local area, whether the well-ordered BM-structure can be obtained homogeneously in the LCO film is still unknown. In general,  $\text{SrCoO}_{2.5}$  and  $\text{SrFeO}_{2.5}$  usually exhibit the BM phase in an ambient atmosphere [9–14], whereas LCO favors the PV structure due to the high oxygen vacancy formation energy ( $\sim 4.02$  eV) [37]. Seeking effective approaches to realize the uniform BM phase of  $\text{LCO}_{2.5}$  becomes a very interesting issue. It will allow a systematic investigation of the special magnetic and transport properties of oxygen-deficient LCO caused by the ordering of oxygen vacancies. In this paper, we report an effective way to tune the crystal structure of epitaxial LCO film. The reversible topotactic phase transition between the PV, BM and other oxygen vacancy-ordered structures are achieved by annealing samples in the vacuum or oxygen atmosphere with an appropriate temperature. We found that the BM LCO is antiferromagnetic, with a Néel temperature around 290 K. The BM phase is more insulating, implying an enhanced charge localization. Interestingly, the BM to PV transition proceeds via two steps; the BM phase transits to an intermediate phase  $\text{La}_3\text{Co}_3\text{O}_8$  before reaching the PV phase. Obviously, the oxygen vacancies adjusting their arrangement in a cooperative way as oxygen atoms fill in.

## Experimental details

LCO thin films (30 nm) were deposited on (001)-oriented  $\text{SrTiO}_3$  (STO) single crystal substrates with the miscut angle  $\leq 0.3^\circ$  by pulsed laser deposition, using a KrF excimer laser with a wavelength of 248 nm and a repetition of 2 Hz.

The laser fluence was  $1.6 \text{ J cm}^{-2}$ . The deposition was carried out at  $700^\circ\text{C}$  in an oxygen environment of 30 Pa. After deposition, the samples were cooled down to room temperature in 100 Pa oxygen with a cooling rate of  $5^\circ\text{C min}^{-1}$ . The film thickness was controlled by the number of laser pulses, which had been carefully calibrated by the technique of small angle x-ray reflectivity.

The surface morphology of the films was measured by an atomic force microscope (AFM, SPI 3800N, Seiko). X-ray diffraction (XRD) patterns of the samples were collected by a Bruker diffractometer (D8 Discover,  $\text{Cu K}\alpha$  radiation). Magnetic measurements were performed on the Quantum-designed vibrating sample magnetometer (VSM-SQUID) in the temperature interval from 10 K to 380 K. Resistance of the films was measured by the Quantum-designed physical property measurement system (PPMS) using the standard four-probe method with an applied current of  $0.1 \mu\text{A}$ .

## Results and discussion

The surface morphology of epitaxial LCO film is performed by AFM, which displays atomically flat surface with a root mean square roughness of  $\sim 0.2 \text{ nm}$  and is measured over an area of  $5 \times 5 \mu\text{m}^2$  (supporting information figure S1 ([stacks.iop.org/JPhysD/53/155003/mmedia](https://stacks.iop.org/JPhysD/53/155003/mmedia))). The thickness of the LCO film is  $\sim 30 \text{ nm}$ , as determined by small angle x-ray reflectivity (supplementary material figure S2). To cause a topotactic phase transition, the LCO films were annealed in different temperature ranging from  $100^\circ\text{C}$  to  $600^\circ\text{C}$  for 60 min in an oxygen atmosphere of  $2 \times 10^{-4} \text{ Pa}$ . To trace phase transition, XRD measurements were performed after each post-annealing, as shown in figure 1(a). The PV structure is the dominated phase when the annealing temperature is lower than  $400^\circ\text{C}$ . In this case, only (001) and (002) peaks are observed in the  $\theta - 2\theta$  curves, without any fractional peaks. Reflections with half-integer indices appear when annealing temperature exceeds  $500^\circ\text{C}$ . Appearance of half-integer peaks in the XRD spectrum indicates the formation of superstructure with doubled lattice constant along the  $c$ -axis. Since the superstructure forms after the introduction of oxygen vacancies into the LCO film, it must have a close relation with the ordering of the oxygen vacancies. As reported, oxygen vacancies in LCO film prefer to form  $\text{CoO}_4$  layers, resulting in dark stripes in lattice image [31–36]. To form a BM-typed superstructure, the most feasible approach is the alternate stacking of the  $\text{CoO}_4$  and  $\text{CoO}_6$  layers. In fact, this kind of superstructure has been observed in the local areas of the LCO film after extracting oxygen ions from the LCO film using electron beam irradiation [35, 36]. Notably, the XRD patterns of our oxygen-deficient LCO films show exactly the same features of those of  $\text{SrCoO}_{2.5}$  and  $\text{SrFeO}_{2.5}$  films which are typical BM phase (supporting information figure S3). Therefore, it's reasonable to believe that the BM-structured  $\text{LCO}_{2.5}$  film is obtained after high-temperature vacuum annealing. The BM structure of  $\text{LCO}_{2.5}$  is stable in ambient atmosphere for several weeks. In fact, the crystal structure of the film begins to change before the appearance of the superstructure. Figure 1(b) is an enlarged view of the

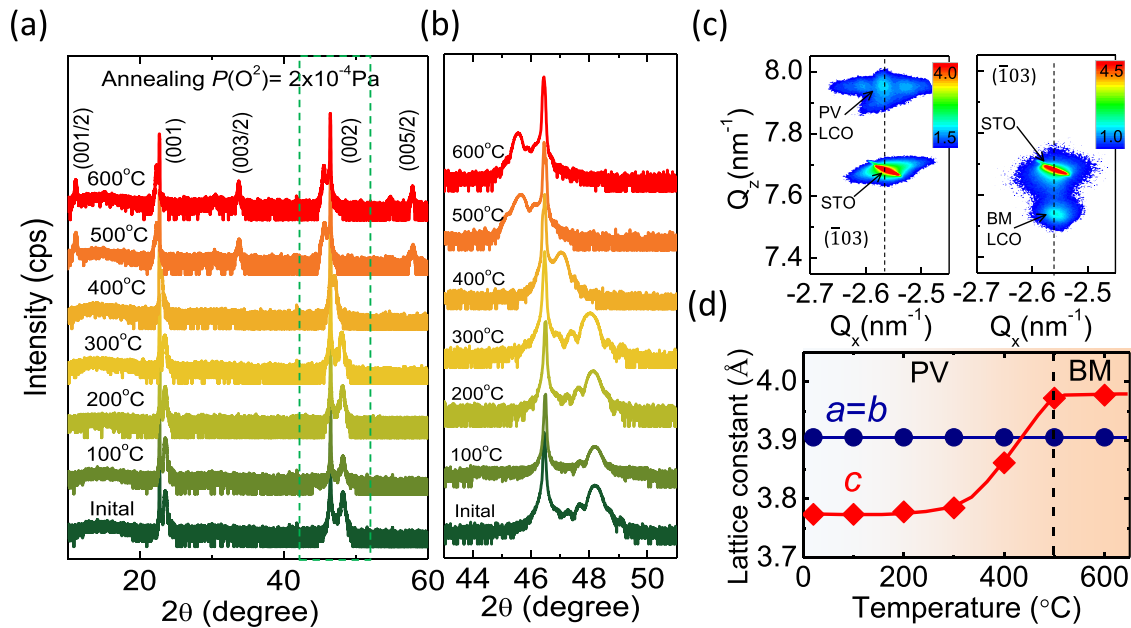


**Figure 1.** (a), (b) X-ray diffraction spectra of the films after a series of post-annealing processes. (c) Reciprocal space maps of LCO (left panel) and LCO<sub>2.5</sub> (right panel) films around asymmetric  $(\bar{1}03)$  reflection. (d) Lattice constants as functions of annealing temperature.

(002) peaks of the films. The (002) peak position is  $\sim 48.05^\circ$  for the sample of 300 °C and  $\sim 47.03^\circ$  for the sample of 400 °C, signifying a lattice expansion along the  $c$ -axis. Obviously, considerable oxygen vacancies enter the lattice at 400 °C, converting Co ions to a lower valence state with a larger ionic radius and expanding the lattice. Despite the significant lattice expansion for the sample of 400 °C, the film still remains to be PV-structured since all diffraction peaks in the corresponding XRD spectrum can be indexed in the PV structure (figure 1(a)). Probably, the distribution of the vacancies in the film is random. Above the annealing temperature of 500 °C, however, the PV to BM transition finishes. The ordering of oxygen vacancies in the film causes a further lattice expansion. As shown in figure 1(b), the (002) peak now appears on the left side of that of STO, i.e. the  $c$ -axis lattice constant of the film has exceeded that of the substrate.

In general, the epitaxial films could be coherently strained by substrate. This is exactly the case of the LCO/STO films. Figures 1(c) are the typical reciprocal space maps of the  $(\bar{1}03)$  reflections for PV LCO and BM LCO<sub>2.5</sub> film, the latter is obtained after annealing at 500 °C. The reflections from the film and the substrate align vertically, indicating that the film is coherently strained by substrate without any lattice relaxations. Based on the data in figures 1(b) and (c), the lattice parameters of the films are deduced. As shown in figure 1(d), the in-plane lattice constant of films is  $a = b = 3.905$  Å, regardless of annealing temperature. In contrast, the out-of-plane lattice constant of the films undergoes a rapid contraction from 500 °C to 300 °C which is also the temperature range for phase transition. Below 300 °C, it is nearly constant, indicating negligible oxygen loss. Increasing annealing temperature further to 600 °C has no obvious effects on lattice parameters.

Remarkably, the topotactic transition is reversible. By tempering the BM LCO<sub>2.5</sub> film in a  $10^5$  Pa oxygen atmosphere

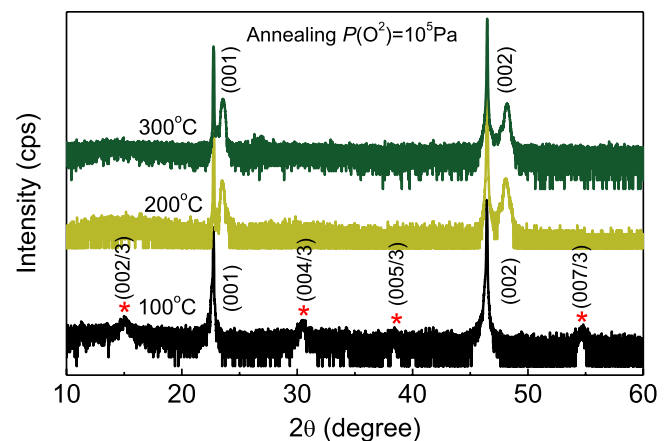


**Figure 2.** The x-ray diffraction of the films under different annealing temperatures in an O<sub>2</sub> atmosphere of  $10^5$  Pa. The sample goes back to the PV state above the annealing temperature of 200 °C. However, an intermediated phase appears when annealing temperature is 100 °C, as marked by the appearance of fractional indices.

for 60 min at 200 °C, we found that the PV structure totally recovers (figure 2). Notably, this temperature is much lower than that required by other BM oxides such as SrCoO<sub>2.5</sub> and SrFeO<sub>2.5</sub> [9–15]. If the annealing temperature is not high, moreover, an intermediate phase with the formula of La<sub>3</sub>Co<sub>3</sub>O<sub>8</sub> appears, which is consist of one CoO<sub>4</sub>-tetrahedra layer sandwiched between two CoO<sub>6</sub>-octahedra layers along the out-of-plane direction [35, 38]. As shown in figure 2, when annealing the sample at 100 °C, distinct XRD spectrum appears. In addition to the excepted (001) reflections, a series of superstructure peaks with the indices of  $(00\frac{l}{3})$  are seen (marked by red stars). The out-of-plane lattice constant is 11.72 Å, three times as large as that of STO. Similar to the BM phase of LCO<sub>2.5</sub>, La<sub>3</sub>Co<sub>3</sub>O<sub>8</sub> is also a metastable phase and it will eventually turn

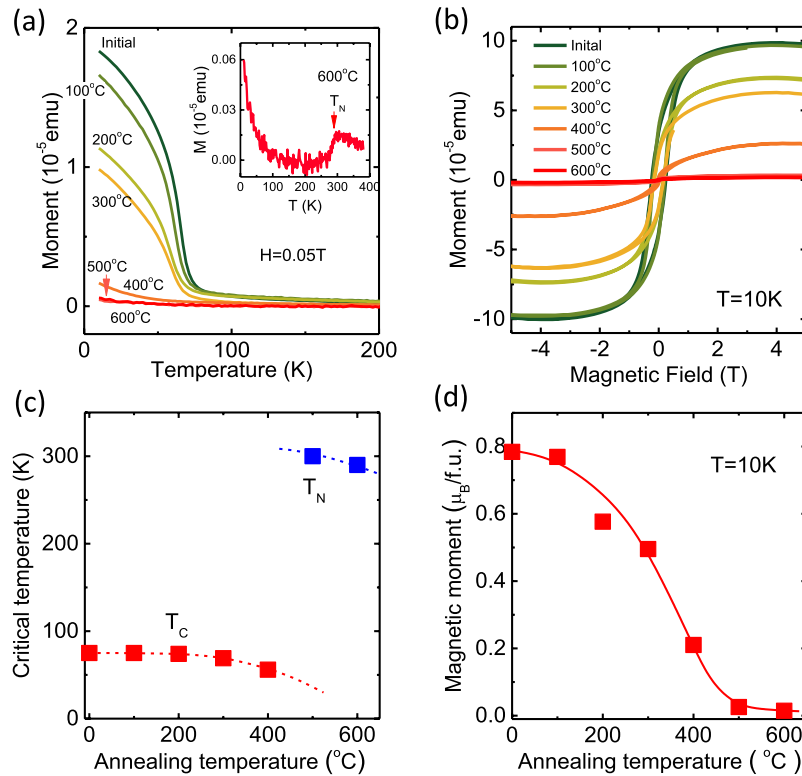


**Figure 3.** (a) Thermomagnetic curves of the films after a series of post-annealing processes. The insert plot is an enlarged view of the results after a post-annealing at 600°. All thermomagnetic measurements were performed at the field-cooling mode with the applied field of  $H = 0.05$  T. (b) Magnetic loops of the film obtained at 10 K. (c) Critical temperature for magnetic transition, depicted as a function of annealing temperature. (d) Saturation magnetization deduced from (b). Dashed and solid lines are guides for the eye.

into the PV phase when exposing to air long enough (supporting information figure S4).

Different from its bulk counterpart, the LCO film is FM when tensely strained [25–29]. It is an interesting question of what behavior will be displayed when oxygen vacancies are incorporated. Figure 3(a) shows the thermomagnetic ( $M$ - $T$ ) curves of the films after each annealing, measured in an applied field of 0.05 T with field-cooling mode. When the annealing temperature is lower than 300 °C, the films exhibit the typical paramagnetic (PM) to FM transition. In this case, magnetization displays a gradual reduction with annealing temperature whereas the Curie temperature remains essentially unaffected. Above the annealing temperature 500 °C, the magnetic signals are rather weak, indicating the disappearance of FM order. Accompanying the disappearance of the FM order, however, a visible cusp emerges in the  $M$ - $T$  curve around 290 K (inset plot in figure 3(a)). This is an indication of the establishment of an AFM order for the BM-LCO<sub>2.5</sub> film, which is similar with the previous results of the phase transition for the SrFeO<sub>3-δ</sub> ( $\delta = 0$ –0.19) single crystals [39]. This result is consistent with the previous results of neutron diffraction which shows that LCO<sub>2.5</sub> is G-type antiferromagnetic (AFM) with a Néel temperature of ~300 K [40]. However, the magnetic moment rapidly increases upon cooling when temperature is below 70 K (inset plot in figure 3(a)), and its temperature dependence obeys the Curie–Weiss law. This suggests the presence of minor Co ions remains in the PM state while most of other Co ions form the AFM order.

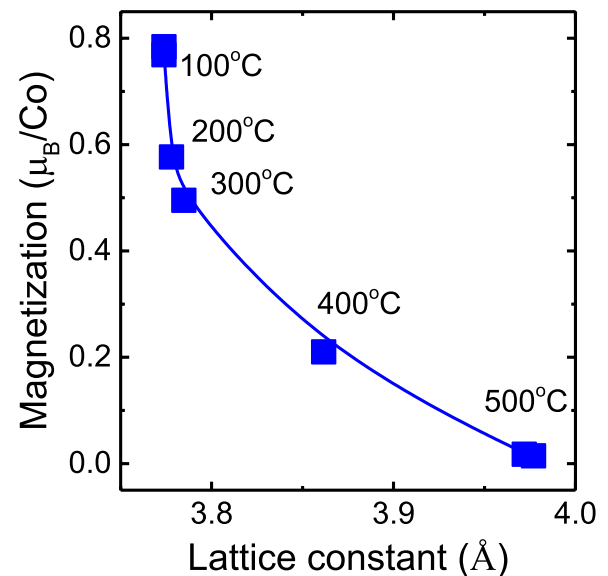


**Figure 4.** Magnetization as a function of lattice constant. A rapid drop in magnetization implies that oxygen may prefer to be formed near HS Co<sup>3+</sup> in the initial stage. The solid line is a guide for the eye.

To trace the variation of magnetic order, in figure 3(b) we show the field dependence of magnetization measured at 10 K after each annealing. The magnetic loops are clear below the annealing temperature of 400 °C. However, the saturation magnetization displays a rapid decrease with annealing

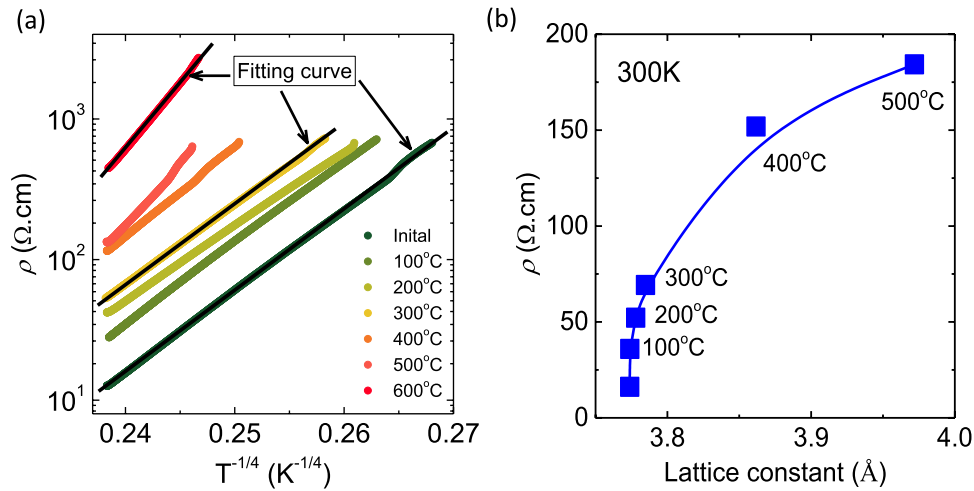


**Figure 5.** (a) Resistivity as a function of temperature, depicted in a semi-logarithmic scale. The linear dependence indicates the transport mechanism of variable-range hopping. Notably, the slope of the resistivity curve considerably inclines from the PV to the BM phase. (b) Resistivity as a function of lattice constant, the data is collected at 300 K. The solid line is a guide for the eye.

temperature. It is  $\sim 0.8 \mu_B/\text{Co}$  in the initial state and  $\sim 0.2 \mu_B/\text{Co}$  after an annealing of 400 °C. As well established [25–29], in LCO about one fourth  $\text{Co}^{3+}$  ions are in HS state. Therefore, the expected saturation magnetization is  $1 \mu_B/\text{Co}$ , close to the observed  $0.8 \mu_B/\text{Co}$ . Quantifying the content of oxygen vacancies in LCO with out-of-plane constant, we can establish a relationship between magnetization and oxygen vacancies. As shown in figure 4, magnetization drops sharply at the beginning of the incorporation of oxygen vacancies. When the content of oxygen vacancies is low, oxygen vacancies may prefer to appear near HS  $\text{Co}^{3+}$  since HS  $\text{Co}^{3+}$  have much larger radius than the LS state [24, 30–34], converting the HS  $\text{Co}^{3+}$  into  $\text{Co}^{2+}$ . This result is consistent with the previous results of x-ray absorption spectrum which shows that oxygen vacancy preferentially convert HS  $\text{Co}^{3+}$  to  $\text{Co}^{2+}$  ions [29]. This will strongly depress the FM super-exchange that occurs between HS  $\text{Co}^{3+}$  ions since the content of HS  $\text{Co}^{3+}$  is low as mentioned above. This explains the rapid decrease of magnetization in the initial stage when oxygen vacancies are introduced. However, oxygen vacancies may prefer to aggregate into chains to reduce formation energy [6–15, 36]. This means that the later oxygen vacancies may prefer to form at adjacent sites of existing oxygen vacancies rather than choosing an isolated site neighboring HS  $\text{Co}^{3+}$ . This will reduce the efficiency of the oxygen vacancy to convert HS  $\text{Co}^{3+}$  ions. As a result, some of the HS  $\text{Co}^{3+}$  ions survive though the content of oxygen vacancies is high. This explains the sizable magnetization of the sample of 400 °C, in which the content of oxygen vacancies could be considerably high. When the annealing temperature exceeds 500 °C, the magnetic loop disappears completely and the AFM order appears. Oxygen vacancies introduce extra electrons that cause a transition from HS  $\text{Co}^{3+}$  to become the  $\text{Co}^{2+}$  which contains half-occupied  $e_g$  orbitals supporting AFM super-exchange [29–32]. We summarize the critical temperature (figure 3(c)) and saturation magnetization (figure 3(d)) as functions of annealing temperature.

Post-annealing also has a strong effect on transport property. The film is insulating in the whole temperature range

investigated and exhibits a tendency towards more resistive states as annealing temperature increases. Figure 5(a) shows the temperature dependence of the resistivity of the LCO film. A careful analysis indicates that the temperature-dependent resistivity obeys the equation  $\rho = \rho_0 \exp[(T_0/T)^{1/4}]$ , i.e., the electronic transport proceeds via variable-range hopping rather than small polaron hopping that is usually observed in hole-doped manganite [41–43], where  $\rho_0$  and  $T_0$  are parameters independent of temperature,  $T_0 \propto \frac{1}{\xi^3}$  with  $\xi$  being a parameter characterizing electron localization. A direct calculation indicates that  $T_0$  is  $\sim 3 \times 10^8$  K for the PV phase. Based on the formula of  $T_0 = 1/k_B \xi^3 g(E_F)$ , the upper limit of the density of state at the Fermi level is  $g(E_F) \sim 6 \times 10^{23} \text{ m}^{-3} \text{ eV}$  adopting a localization length of 4  $\text{\AA}$ , where  $k_B$  is the Boltzman constant.  $g(E_F)$  is lower by four orders of magnitude than that in hole-doped manganite which show a metallic behavior. Surprisingly, all PV-structured (BM-structured) samples exhibit essentially the same  $\ln \rho - T^{-1/4}$  slope though the content of oxygen vacancies in the samples is different. This is a general feature and also observed in LCO/STO superlattices grown on STO (not shown). This result implies that  $\xi^3 g(E_F)$  is independent of the content of oxygen vacancies. However, the  $\ln \rho - T^{-1/4}$  curve strongly upward shifts in the initial stage of the incorporation of oxygen vacancies. Notably, this behavior exactly corresponds to the drastic decrease of saturation magnetization shown in figure 4. Possibly, HS  $\text{Co}^{3+}$  ions are strongly involved in the process of variable-range hopping, because the smaller electron excitation energy from the  $\sigma$ -like band of HS  $\text{Co}^{3+}$  than that of  $\pi$ -like band of LS  $\text{Co}^{3+}$  ions [32, 41]. For the BM phase,  $T_0$  takes a value of  $\sim 2 \times 10^9$  K, larger than that of the PV phase by nearly an order of magnitude. Correspondingly,  $g(E_F)$  becomes  $\sim 9 \times 10^{22} \text{ m}^{-3} \text{ eV}$ . As expected, change in crystal structure strongly affects the band structure of the sample, resulting in more difficult electron hopping. Quantifying the content of oxygen vacancies in LCO with out-of-plane constant, we can establish a relationship between resistivity

and oxygen vacancies. As shown in figure 5(b), resistivity increase slowly at the beginning of the incorporation of small oxygen vacancies. However, the resistivity increases rapidly as annealing temperature ranging from 300 °C to 500 °C, corresponding to the formation of considerable oxygen vacancies. Such oxygen vacancies cause  $\text{Co}^{3+}$  ions to  $\text{Co}^{2+}$  ions, which favor electron localization and enhance the resistivity of the LCO film [29–35].

## Conclusion

In summary, a reversible topotactic phase conversion from PV structure to BM structure and vice versa is achieved in epitaxial LCO thin films. Remarkably, an intermediate  $\text{La}_3\text{Co}_3\text{O}_8$  phase is captured in the evolution process from the BM to the PV phases. This result reveals the rich phase structures of LCO. Accompanying phase transition, the magnetic properties and transport properties exhibit dramatic variations. The PV phase is FM and less resistive whereas the BM phase is AFM and highly resistive. The Curie temperature is ~75 K for the PV phase while the Néel temperature is ~290 K for the BM phase. The reversible control of crystal structure via introducing ordered oxygen vacancies provides an effective approach to tune the physical properties of the LCO-based oxides, which has potential application in the fields of resistive switching memories, redox catalysts, high ionic conductors, electrochemical sensors.

## Acknowledgments

This work has been supported by the National Basic Research of China (Nos. 2016YFA0300701, 2017YFA0206300, 2017YFA0303601 and 2018YFA0305704), the National Natural Science Foundation of China (Nos. 11520101002, 51590880, 11674378, 11934016 and 51972335), and the Key Program of the Chinese Academy of Sciences.

## ORCID iDs

Jirong Sun  <https://orcid.org/0000-0003-1238-8770>

## References

- [1] Fister T T, Fong D D, Eastman J A, Baldo P M, Highland M J, Fuoss P H, Balasubramaniam K R, Meador J C and Salvador P A 2008 *Appl. Phys. Lett.* **93** 151904
- [2] Biegalski M D, Crumlin E, Belianinov A, Mutoro E, Shao-Horn Y and Kalinin S V 2014 *Appl. Phys. Lett.* **104** 161910
- [3] Zhang J S, Zhao Z J, Li J B, Jin H B, Rehman F, Chen P W, Jiang Y J, Chen C X, Cao M S and Zhao Y J 2017 *ACS Appl. Mater. Interfaces* **9** 27135
- [4] Zhang J et al 2018 *Nat. Commun.* **9** 1923
- [5] Zhang J E et al 2018 *ACS Appl. Mater. Interfaces* **10** 40951
- [6] Ferguson J D, Kim Y, Kourkoutis L F, Vodnick A, Woll A R, Muller D A and Brock J D 2011 *Adv. Mater.* **23** 1226
- [7] Yao L D, Inkinen S and van Dijken S 2017 *Nat. Commun.* **8** 14544
- [8] Cao L, Petravic O, Zakalek P, Weber A, Rucker U, Schubert J, Koutsoubas A, Mattauch S and Brückel T 2019 *Adv. Mater.* **31** 1806183
- [9] Jeon H, Choi W S, Freeland J W, Ohta H, Jung C U and Lee H N 2013 *Adv. Mater.* **25** 3651
- [10] Jeon H et al 2013 *Nat. Mater.* **12** 1057
- [11] Lu N P et al 2017 *Nature* **546** 22389
- [12] Khare A et al 2017 *Adv. Mater.* **29** 1606566
- [13] Cui B, Werner P, Ma T P, Zhong X Y, Wang Z C, Taylor J M, Zhuang Y C and Parkin S S P 2016 *Nat. Commun.* **3** 3055
- [14] Song J H et al 2019 *Phys. Rev. Mater.* **3** 045801
- [15] Inoue S, Kawai M, Ichikawa N, Kageyama H, Paulus W and Shimakawa Y 2010 *Nat. Chem.* **2** 213
- [16] Cai Z H, Kuru Y, Han J W, Chen Y and Yildiz B 2011 *J. Am. Chem. Soc.* **133** 17696
- [17] Kim Y M et al 2012 *Nat. Mater.* **11** 888
- [18] Kalinin S V and Spaldin N A 2013 *Science* **341** 858
- [19] Mefford J T, Rong X, Abakumov A M, Hardin W G, Dai S, Kolpak A M, Johnston K P and Stevenson K J 2016 *Nat. Commun.* **7** 11053
- [20] Acharya S K et al 2016 *ACS Appl. Mater. Interfaces* **8** 7902
- [21] Wang X Y, Huang K K, Yuan L, Li S, Ma W, Liu Z Y and Feng S H 2018 *ACS Appl. Mater. Interfaces* **10** 28219
- [22] Maris G, Ren Y, Volotchaev V, Zobel C, Lorenz T and Palstra T T M 2013 *Phys. Rev. B* **67** 224423
- [23] Haverkort M W et al 2006 *Phys. Rev. Lett.* **97** 176405
- [24] Podlesnyak A, Streule S, Mesot J, Medarde M, Pomjakushina E, Conder K, Tanaka A, Haverkort M W and Khomskii D I 2006 *Phys. Rev. Lett.* **97** 247208
- [25] Merz M, Nagel P, Pinta C, Samartsev A, Loehneysen H V, Wissinger M, Uebe S, Assmann A, Fuchs D and Schuppler S 2010 *Phys. Rev. B* **82** 174416
- [26] Mehta V and Suzuki Y 2011 *J. Appl. Phys.* **109** 07D717
- [27] Seo H, Posadas A and Demkov A A 2012 *Phys. Rev. B* **86** 014430
- [28] Yang H W, Zhang H R, Li Y, Wang S F, Shen X, Lan Q Q, Meng S, Yu R C, Shen B G and Sun J R 2014 *Sci. Rep.* **4** 06206
- [29] Meng D C et al 2018 *Proc. Natl Acad. Sci. USA* **115** 2873
- [30] Liu G J, Li X T, Wang Y Q, Liang W S, Liu B, Feng H L, Yang H W, Zhang J and Sun J R 2017 *Appl. Surf. Sci.* **425** 121
- [31] Choi W S et al 2012 *Nano Lett.* **12** 4966
- [32] Biskup N, Salafranca J, Mehta V, Oxley M P, Suzuki Y, Pennycook S J, Pantelides S T and Varela M 2014 *Phys. Rev. Lett.* **112** 087202
- [33] Kwon J H, Choi W S, Kwon Y K, Jung R J, Zuo J M, Lee H N and Kim M 2014 *Chem. Mater.* **26** 2496
- [34] Mehta V V, Biskup N, Jenkins C, Arenholz E, Varela M and Suzuki Y 2015 *Phys. Rev. B* **91** 144418
- [35] Jang J H et al 2017 *ACS Nano* **11** 6942
- [36] Guan X X et al 2019 *Inorg. Chem.* **58** 13440
- [37] Jia T, Zeng Z, Zhang X L, Ohodnicki P, Chorpene B, Hackett G, Leksea J and Duan Y H 2019 *Phys. Chem. Chem. Phys.* **21** 20454
- [38] Hansteen O H, Fjellvåg H and Hauback B C 1998 *J. Mater. Chem.* **8** 2081
- [39] Lebon A, Adler P, Bernhard C, Boris A V, Pimenov A V, Maljuk A, Lin C T, Ulrich C and Keimer B 2004 *Phys. Rev. Lett.* **92** 037202
- [40] Hansteen O H, Fjellvåg H and Hauback B C 1998 *J. Solid State Chem.* **141** 411
- [41] Senarisrodriguez M A and Goodenough J B 1995 *J. Solid State Chem.* **116** 224
- [42] Coey J M D, Viret M and Ounadjela K 1995 *Phys. Rev. Lett.* **75** 3910
- [43] Viret M, Ranno L and Coey J M D 1997 *Phys. Rev. B* **58** 11519